MicroRNA-495 Regulates Collateral Formation And Predicts Myocardial Perfusion In Coronary Chronic Total Occlusion Disease

Wei Gao
Zhongshan Hospital Fudan University
Runda Wu
Zhongshan Hospital Fudan University
Jie Yuan
Zhongshan Hospital Fudan University
Youming Zhang
zhongshan hospital fudan university qingpu branch
Guobing Liu
Zhongshan Hospital Fudan University
Jianhui Zhang
Zhongshan Hospital Fudan University
Jian Yang
Zhongshan Hospital Fudan University
Chenguang Li
Zhongshan Hospital Fudan University
Hongcheng Shi
Zhongshan Hospital Fudan University
Haibo Liu
Zhongshan hospital fudan university qingpu branch
Junbo Ge (jbge@zs-hospital.sh.cn)
Zhongshan Hospital Fudan University https://orcid.org/0000-0002-9360-7332

Research Article

Keywords: MicroRNA-495, coronary artery disease, chronic total occlusion, angiogenesis

Posted Date: July 19th, 2021

DOI: https://doi.org/10.21203/rs.3.rs-661498/v1

Abstract

How miRNAs play a role in collateral formation of chronic total occlusion (CTO) patients and in predicting myocardial perfusion has not been investigated. In this study, we screened circulating miRNAs in CTO and stable coronary artery disease patients using high-throughput sequencing and found 42 differential expressed miRNAs, including miR-329, miR-494 and miR-495, which belong to 14q32 miRNAs gene cluster. The down regulation of miR-329, miR-494 and miR-495 was confirmed in an independently larger cohort. Then in vitro and in vivo study, we demonstrated that miR-495 inhibited angiogenesis and collateral formation through Notch1 pathway. Finally we came back to a clinical view and found that miR-329, miR-494 and miR-495 were able to predict whether myocardial perfusion can be improved in CTO patients after revascularization. These data indicate that miRNAs are involved into the collateral formation of CTO patients and could be potentially biomarkers to help individualise therapeutic decisions.

Introduction

Cardiovascular disease remains the leading cause of death worldwide. Among patients with known coronary artery disease (CAD), the prevalence of chronic total occlusions (CTO) is between 30 to 50% [1, 2]. A CTO is defined as a native coronary artery with complete vessel occlusion, and an estimated occlusion duration of not less than 3 months. Despite the high prevalence, only part of them was treated by revascularization [3]. Guidelines recommended that revascularization can be considered if an ischemia reduction in the CTO territory and/or the relief of angina symptoms can be expected [4]. Thus, other methods to improve myocardial perfusion and predictors to screen potential candidates for revascularization are of interest of researchers.

A specific characteristic of CTO is collateral circulation, which can be seen in almost all of these patients [5]. Although well-developed collaterals can not provide sufficient blood supply [6], they have been shown to be related with better ventricular function [7, 8]. According to the collateral size and filling, collateral vessels can be classified by collateral connection (CC) grade [9] and Rentrop's grade [10]. Arteriogenesis and angiogenesis are two major processes of collateral growth [11]. The underlying mechanisms were complex, including shear stress and molecular and cellular response to hypoxia. MicroRNAs (miRs) are small non-coding RNA molecules and play an important role in angiogenesis. The roles of miRs have been thoroughly investigated in stable CAD [12] and myocardial infarction [13]. However, expression profile of miRs in CTO patients has not been studied.

In this study, we screened circulating miRs in CTO and stable CAD patients using high-throughput sequencing and found 42 differential expressed miRs, including miR-329, miR-494 and miR-495. These three significantly down-regulated miRs belong to the 14q32 miR gene cluster, which was first discovered in 2004 [14]. Then it was demonstrated that inhibition of individual 14q32 miRs leads to improvements in post-ischemic blood flow recovery in mice [15]. Previous studies found miR-329 and miR-494 suppresses

angiogenesis by targeting CD146 [16] and BMPER [17], respectively. However, the underlying mechanism of miR-495 inhibiting angiogenesis remains unclear.

We used www.targetscan.org to predict targets of miR-495 and found Notch1 was one of the potential targets. We then tested the hypothesis that miR-495 inhibited angiogenesis by targeting Notch1 pathway. In human umbilical vein endothelial cells (HUVEC) study, we found miR-495 inhibited cell migration and tuber formation through activating NOTCH1. In limb ischemia mice study, we showed NOTCH1 was target of miR-495, which inhibited collateral formation. In human study, miR-329, miR-494 and miR-495 were able to predict those patients who have myocardial perfusion improvement detected by Single-photon emission computed tomography (SPECT) after revascularization.

Materials And Methods

Patient selection

A total of 5 CAD and 4 CTO patients were selected for miRNA sequencing. The criteria were as follows: male, aged from 45 to 65 years old, no left ventricular dysfunction, no myocardial infarction history, no tumor history, normal liver and renal function. The CAD patients were all presented with left anterior descending (LAD) stenosis of 70-90%. The CTO patients were all LAD-CTO and presented with collateral circulation from left circumflex (LCX) or right coronary artery (RCA). Another cohort of 68 patients was selected to verify expression of miRs. They include 22 CAD and 46 CTO patients > 18 years of age. The CAD patients had a 50-90% stenosis of at least one main vessel (LAD, LCX or RCA). The CTO was defined as completely occluded coronary arteries with Thrombolysis In Myocardial Infarction 0 flow with an estimated duration of at least 3 months[18]. The exclusive criteria were: symptomatic peripheral arterial disease, recent ST-segment elevation myocardial infarction, decompensated heart failure, any concomitant inflammation or infectious diseases, neoplastic diseases, and severe liver and kidney dysfunction. The cardiac history and risk factors of all patients were documented. A venous blood sample was collected for all patients upon admission (within 24 hours) and before percutaneous coronary intervention (PCI) procedure. The blood sample was centrifuged at 1,500 g for 10 min to precipitate blood cells and plasma was then frozen at -80℃ until use.

This study was approved by the medical ethics committee of Zhongshan Hospital. Informed consent was obtained from all patients. All procedures performed in studies involving human participants were in accordance with the ethical standards of the institutional and/or national research committee and with the Helsinki declaration and its later amendments.

Collateral grading

Angiograms were reviewed by an experienced angiographer who was blinded to the miRNA analysis. Collateral vessels were classified by collateral connection (CC) grade: CC0: no continuous connection between donor and recipient artery; CC1: continuous, threadlike connection (diameter ≤ 0.3 mm); CC2: continuous, small, side-branch-like size of the collateral throughout its course (diameter ≥ 0.4 mm).

MiRNA Sequencing

Small RNAs were isolated from the total RNA of patients' plasma. The high-tthroughput sequencing was performed by WuXi NextCODE company (Shanghai, China) [19, 20].

Cell Culture and Transfection

Human umbilical vein endothelial cells (HUVEC) were purchased from ATCC and cultured as described previously [21]. Briefly, Cells were cultured with a special medium ECM (ScienCell, San Diego, CA, USA). For intervention experiments, VEGF was purchased from Peprotech (USA) and added into medium at a concentration of 10 or 20ng/ml for 24 hours. MiR-495 mimics (50nM, 5'-AAACAAACAUGGUGCACUUCUU-3'), inhibitors (100nM, 5'-AAGAAGUGCACCAUGUUUGUUU-3') and NC (50nM, 5'-CAGUACUUUUGUGUAGUACAA-3') were transfected into HUVECs with Lipo3000 according to the manufacturer's instructions. Notch1 expression was knocked down using Notch siRNA (siNotch1 #1, 5'-CCAACUGCCAGACCAACAUTT-3'; siNotch1 #2, 5'- GGAUCCACUGUGAGAACAATT-3'). All of these oligos were purchased from GenePharma, China.

Measurement of HUVEC Migration and tube formation

HUVEC transwell migration assay was carried out using chambers with filters (pore size of 8-um), coated with Matrigel (BD Biosciences). The cells (1*10^5 cells per well) were seeded into the upper chamber and invasive cells was harvested after incubation for 48 h. Wound healing assay was also performed to evaluate the migration ability. Cells were cultured in 6-well plates to reach 90% confluence. The cell monolayers were scraped with a 100-ul pipette tip, washed twice with PBS, and cultured for 24 h before photographed. For tube formation study, HUVECs (2*10^4 cells/well) were seeded onto Matrigel. Cells were microscopically recorded for the formation of tube-like structures 8 h later. For NC or mimics group, 10ng/ml VEGF was added.

Reverse Transcription-PCR

Total RNA was extracted using TRIzol reagent (Invitrogen; Thermo Fisher Scientific, Inc.) from cells, plasma or tissues according to manufacturer's protocol. The miRNA from each sample was quantified by SYBR Premix Ex Taq qRT-PCR assays (TaKaRa, Japan). Real-time PCR was performed on an ABI 7500 real-time PCR system. The relative expression levels of the miRNAs were normalized to that of U6 by using the 2-ΔΔCq cycle threshold method [22].

Western Blot Analysis

Cultured cells or tissues were harvested and lysed in RIPA buffer supplemented with complete protease inhibitor cocktail tablets. Cell debris was removed by centrifugation at 12,000 rpm for 30 min. Then the lysates were separated by SDS-PAGE gels, transferred to PVDF membranes (Bio-Rad), and incubated with the relevant antibodies as indicated. Antibody against NOTCH1 was purchased from Abcam.

Murine Hindlimb Ischemia Model

This study was approved by the Institutional Review Board of the Zhongshan Hospital, Fudan University and Shanghai Institutes for Biological Sciences and were conducted in conformity with the Public Health Service Policy on Humane Care and Use of Laboratory Animals. Male C57BL/6 mice (8-10 week-old) were used for hindlimb ischemia model. Briefly, the mice were anesthetized with pentobarbitol sodium (0.5%, 50 mg/kg) by intra-peritoneal injection, and the surgical procedures were performed under sterile conditions. A vertical longitudinal incision was made in the left hindlimb, and the femoral artery and its branches were then dissected and ligated.

Transfection in vivo

MiR-495 NC, ago and antago oligonucleotide were purchased from Ribobio, China. Male C57BL/6 mice received miR-495 NC (5nM), agomiR-495 (5nM) and antagomiR-495 (10nM) by multi-point injections in the left adductors or gastrocnemius immediately after the operation.

Hindlimb blood flow measurement

Hindlimb blood flow was measured by the imaging device with laser Doppler perfusion imaging on days 1, 3, 7 and 18 after operation. Mice were anesthetized and placed on a 37 °C heating plate for 5 minutes. Blood flow was measured from scanning images, and the perfusion ratio of ischemic limbs were quantified by averaging relative units of flux from the knee to the toe compared with non-ischemic limbs (PIMsoft Software by Perimed Med, Sweden) [23].

Immunofluorescence Assay

Immunofluorescence assay was conducted as previously described [21]. Briefly, the adductor muscles were harvested at the 3rd day after femoral ligation. The mid-zone of the muscles was trimmed. Samples were embedded in OCT compound and frozen at-80°C. Serial cryostat sections were prepared using a Lab-Tek tissue processor (Leica, Solms, Germany). The sections were stained with CD31 (Abcam, ab222783) and DAPI. Images were acquired on an upright Leica SP8 confocal microscope.

SPECT of CTO patients

SPECT imaging was performed using a single-day rest/stress imaging protocol as previously described [24]. Briefly, for rest imaging, prescanning was performed after the administration of an initial dose of approximately 1 mCi MIBI. Full scanning was started immediately after the injection of the remaining dose of approximately 15 mCi MIBI, and dynamic images were acquired in list mode for over 6 minutes. Following the rest dynamic scanning, rest perfusion scanning was performed. For stress imaging, pharmacological stress was induced with an intravenous infusion of adenosine triphosphate (ATP) disodium at a rate of 140 $ug \cdot kg^{-1} \cdot min^{-1}$ for 5 minutes, and 25 mCi MIBI was injected 3 minutes later from the start of ATP injection, followed by dynamic image acquisition for over 6 minutes. After that, stress

perfusion scanning was acquired. Image acquisition was achieved with a D-SPECT cardiac scanner (Spectrum Dynamics, Caesarea, Israel).

Statistical Analyses

The data are presented as means ± SD. In comparisons of 2 groups, the 2-tailed Student's t test was used for parametric data, and the Mann-whitney U test for non-parametric data. For all statistical analyses, significance was accepted at the 95% confidence level ($P < 0.05$). Calculation was performed with the GraphPad Prism 6 software package.

Results

Circulating miR-329, miR-494 and miR-495 were down-regulated in chronic total occlusions patients

MiRNA sequencing was performed in 5 CAD and 4 CTO patients. As shown in Fig. 1A, a total of 42 differential expressed miRs were identified (fold change > 2.5). We noticed that miR-329, miR-494 and miR-495 belong to the 14q32 miR gene cluster and they were all significantly down-regulated in CTO patients. We then determined the expression of these 3 miRs in another cohort of 68 male patients, including 22 CAD patients and 46 CTO patients. The results showed miR-329, miR-494 and miR-495 were indeed down-regulated in CTO patients (Fig. 1B). The CTO patients were divided into 2 groups according to poor CC (N = 17, CC = 0 or 1) and good CC (N = 27, CC = 2) group. MiR-329, miR-494 and miR-495 were found to be down regulated in good CC group (Fig. 1C). These results showed that miR-329, miR-494 and miR-495 were down-regulated in CTO patients and might be involved in collateral formation. Since the mechanisms of miR-329 and miR-494 in angiogenesis were demonstrated by previous studies [16, 17], we investigated the role of miR-495 in next experiments.

MiR-495 inhibits angiogenesis through NOTCH1 pathway in endothelial cells

First, we investigated miR-495 expression in human umbilical vein endothelial cells (HUVEC). After being treated with VEGF (10 or 20 ng/mL), miR-495 expression was significantly inhibited (Fig. 2A). Then we investigated the role of miR-495 in angiogenesis of HUVEC. As shown in Fig. 2B and 2C, transwell migration study found miR-495 mimics inhibited cell migration and miR-495 inhibitor increased cell migration. MiR-495 mimics inhibited tube formation and miR-495 inhibitor increased tube formation (Fig. 2D and 2E). Cell wound scratch assay showed similar results (Fig. 2F and 2G).

We used www.targetscan.org to predict targets of miR-495 and found Notch1 was one of the potential targets. We treated HUVEC with VEGF and found Notch1 expression was elevated (Fig. 3A). Then we confirmed that miR-495 mimics inhibited Notch1 expression and miR-495 inhibitor increased Notch1 expression (Fig. 3B). To assess the role of Notch1 in the association between miR-495 and angiogenesis, we constructed two Notch1 siRNAs to interfere Notch1 expression. As shown in Fig. 3C, both siNotch1 #1 and siNotch1 #2 successfully alleviated the increased expression of Notch1 induced by miR-495 inhibitor. HUVEC were then treated with miR-495 inhibitor and Notch1 siRNAs. Tube formation and wound scratch assay showed that miR-495 inhibitor induced angiogenesis of HUVEC was alleviated by Notch1 siRNAs

(Fig. 4A-B). These results demonstrated miR-495 inhibits angiogenesis through NOTCH1 pathway in endothelial cells.

Inhibition of MiR-495 increases angiogenesis in mice after hindlimb ischemia

To explore the role of miR-495 in angiogenesis in mice, we performed hindlimb ischemia study. After left femoral artery ligation, the blood flow in ischemia hindlimbs measured by laser Doppler perfusion began to recover obviously on day 3 (Fig. 5A). Meanwhile, plasma miR-495 expressions after hindlimb ischemia were determined at different time points. We found miR-495 was significantly down expressed one day after hindlimb ischemia (Fig. 5B). From day 3 to day 14, its expression gradually recovered to nearly normal level (Fig. 5C-F). Notch1 has been showed, as target of miR-495, to be involved in angiogenesis in previous HUVEC experiments. After ligation, miR-495 antago and miR-495 ago were injected into ischemic muscle. Then we detected expression of Notch1 and found that antagomiR-495 increased Notch1 expression and agomiR-495 decreased Notch1 expression (Fig. 5G-H). These data demonstrated miR-495 was down-regulated after hindlimbs ischemia and Notch1 was the target of miR-495.

To investigate whether miR-495 play a role in ischemia-mediated angiogenesis in the hindlimb, the adductor muscles of control, miR NC, agomiR-495 and antago miR-495 treated mice were stained for CD31 to visualize capillary formation. The results showed the angiogenesis after ischemia was enhanced by antagomiR-495 and inhibited by agomiR-495 (Fig. 6A). Blood flow study confirmed this phenomenon (Fig. 6B).

Expressions of miR-329, miR-494 and miR-495 were associated with myocardial perfusion improvement after revascularization

SPECT has been widely used to assess myocardial perfusion in CAD, including CTO patients. Previous study demonstrated a lacking relationship between the collateral state and myocardial perfusion in CTO patients, indicating that impaired myocardial perfusion presented in those patients with angiographically well-developed collateral arteries [25]. In this preliminary study, 27 patients underwent SPECT and we investigated the association between miRs expression and myocardial perfusion. We divided these patients into 2 groups according expressions of miR-329, miR-494 and miR-495. The results showed that ischemic areas were not different between groups (Fig. 7A). We then divided them into 2 groups according to whether stress-induced reversible perfusion deficits present. Expressions of miR-329, miR-494 and miR-495 were not different between 2 groups (Fig. 7B). Of these 27 patients, 20 underwent a second SPECT after successful revascularization of occluded artery. A total of 10 patients had improvement of myocardial perfusion after revascularization and another 10 did not have improvement (Fig. 7C). The patients were divided into 2 groups according to whether myocardial perfusion was improved. We found that expressions of miR-329, miR-494 and miR-495 were significantly lower in patients with improved myocardial perfusion than those without (Fig. 7D). Receiver operating characteristic (ROC) curve and area under the curve (AUC) were used to evaluate predictive value of miR-329, miR-494 and miR-495 expressions for myocardial perfusion improvement. The AUC of miR-329, miR-494 and miR-495 was 0.80, 0.68 and 0.69, respectively (Fig. 7E-G). These data indicated that expressions

of miR-329, miR-494 and miR-495 were associated with myocardial perfusion improvement after revascularization. MiR-329, miR-494 and miR-495 are potentially biomarkers to guide revascularization strategy for CTO patients.

Discussion

This is the first study to investigate different expression profiles of miRNAs in CTO and CAD patients. We found a set of differential expressed miRNAs, including the 14q32 miR gene cluster, which were miR-329, miR-494 and miR-495. These 3 miRs were showed to be related to collateral formation in CTO patients. We then demonstrated that miR-495 regulates angiogenesis through NOTCH1 pathway in vitro and in vivo studies. A small group of CTO patients underwent single- photon emission computed tomography (SPECT) before and after PCI therapy. MiR-329, miR-494 and miR-495 were able to predict whether myocardial perfusion can be improved after PCI.

The specific characteristic of CTO is collateral circulation, which attracted lot of attention in CTO research. Clinical practioners focused on whether the collateral circulation is sufficient to provide blood supply and can predict clinical prognosis. Basic researchers were interested in how it takes shape and what the impact factors are.

In a preliminary study, we explored the relationship between thrombospondin-1, endostatin, angiopoietin-2, and coronary collateral development in patients with CTO [26]. We found circulatory endostatin may be a useful biomarker for coronary collateral development and potential target for therapeutic angiogenesis. Other studies also found some collateral associated factors, such as gamma glutamyl transferase [27], neutrophil/lymphocyte ratio [28, 29], C-reactive protein [30], mimecan [31], angiogenin and osteopontin [32]. However, none of above studies further investigated these factors' mechanisms of influencing collateral circulation nor their clinical significance.

A previous study identified some differentially expressed miRs in CTO patients with well or poorly developed collateral circulation [33]. There was a big difference between their results and this currents study. It might due to different participants: the previous study focused on CTO patients with well or poorly developed collateral circulation; our current study enrolled CTO and CAD patients. In the past decade, the role of miRs in the regulation of both angiogenesis and arteriogenesis has been demonstarted. As discussed in a recent review, miRs can be both anti-angiogenic and proangiogenic [34]. The 14q32 miR gene cluster, including miR-329, miR-487b, miR-494 and miR-495, were of interest to researchers. Gene-Specific Oligonucleotides (GSO) were used to systemically inhibit these miRs in hind limb ischemia models and improved recovery of perfusion was observed [15]. In this current study, we observed a down-regulated expression of miR-495 in CTO patients and then showed that it inhibited angiogenesis through NOTCH1 pathway.

There is a potential for therapeutic modulation of miRs. A long-acting siRNA targeted towards Proprotein Convertase Subtilisin–Kexin type 9 (PCSK9) has been showed to lower LDL levels [35] and reduce cardiovascular risk [36]. Varying grades of collaterals can be found in CTO patients and well developed

collaterals have been shown to be related with better ventricular function. Although miR-based therapeutics were successful in improving perfusion in animal models, they have not been studied in CTO disease. With an ever increasing interest in the management of CTO in humans, investigation of animal CTO models also attracted researchers' attention [37]. A reliable and reproducible animal model may be helpful for therapeutic experiments. In this current study, we used hindlimb ischemia mice model to investigate therapeutic effect of miR-495 and found some inspiring results. Future studies in CTO models were warranted.

SPECT has been widely accepted as the reference standard for ischemia and viability testing in CTO patients. A previous study divided CTO patients who successfully underwent PCI into 3 groups according to SPECT fusion imaging: no severe cardiac perfusion defects, reversible cardiac perfusion defects and fixed cardiac perfusion defects. The results showed SPECT were helpful for distinguishing patients who benefits most from PCI therapy [38]. As far as we know, no biomarkers have been developed to predict myocardial perfusion improvement after PCI in CTO patients. We for the first time investigated the association between miRs expression and SPECT fusion imaging. We did not find an association between miRs expressions and ischemic area in SPECT imaging. However, we showed that miR-329, miR-494 and miR-495 expressions were lower in those perfusion improved patients after revascularization, indicating that myocardial ischemia present in these patients and revascularization may benefit. Further clinical study with large sample was guaranteed to investigate clinical significance of miR-329, miR-494 and miR-495 expressions in CTO patients.

In conclusion, for the first time to our knowledge, we identified that circulating miR-329, miR-494 and miR-495 were substantially down-regulated in CTO patients, and especially in those patients with good collateral formation. In vitro and in vivo study, we confirmed that miR-495 inhibited angiogenesis and collateral formation through Notch1 pathway. Then we came back to a clinical view and found that miR-329, miR-494 and miR-495 were able to predict whether myocardial perfusion can be improved in CTO patients after revascularization. Above all, we showed the underlying molecular mechanism of miRs involving into angiogenesis and their translational value in CTO patients.

Declarations

Acknowledgments:

None.

Funding

This study was supported by National Natural Science Foundation of China (No. 81900305 to W.G., No. 81770350 to H.L. and No. 81870200 to J.Y.) and Grants of Zhongshan hospital (No.2019ZSYXQN25 to W.G.).

Author contributions:

W.G. designed and performed experiments, conducted the clinical trial, analyzed the data, and wrote the manuscript. R.W. and J.Y. performed in vitro/in vivo experiments and analyzed the data. Y.Z., J.Z. and J.Y. performed experiments. G.L., C.L and H.S. performed SPECT and analyzed the data. H.L. and J.G. designed and supervised the study.

Competing interests:

None.

Data and materials availability:

Materials are available upon request from the corresponding author.

References

[1] R.D. Christofferson, K.G. Lehmann, G.V. Martin, N. Every, J.H. Caldwell, S.R. Kapadia (2005) Effect of chronic total coronary occlusion on treatment strategy. Am J Cardiol 95(9): 1088-91.

[2] V.S. Srinivas, M.M. Brooks, K.M. Detre, S.B. King, 3rd, A.K. Jacobs, J. Johnston, D.O. Williams (2002) Contemporary percutaneous coronary intervention versus balloon angioplasty for multivessel coronary artery disease: a comparison of the National Heart, Lung and Blood Institute Dynamic Registry and the Bypass Angioplasty Revascularization Investigation (BARI) study. Circulation 106(13): 1627-33.

[3] P. Fefer, M.L. Knudtson, A.N. Cheema, P.D. Galbraith, A.B. Osherov, S. Yalonetsky, S. Gannot, M. Samuel, M. Weisbrod, D. Bierstone, J.D. Sparkes, G.A. Wright, B.H. Strauss (2012) Current perspectives on coronary chronic total occlusions: the Canadian Multicenter Chronic Total Occlusions Registry. J Am Coll Cardiol 59(11): 991-7.

[4] S. Windecker, P. Kolh, F. Alfonso, J.P. Collet, J. Cremer, V. Falk, G. Filippatos, C. Hamm, S.J. Head, P. Juni, A.P. Kappetein, A. Kastrati, J. Knuuti, U. Landmesser, G. Laufer, F.J. Neumann, D.J. Richter, P. Schauerte, M. Sousa Uva, G.G. Stefanini, D.P. Taggart, L. Torracca, M. Valgimigli, W. Wijns, A. Witkowski (2014) 2014 ESC/EACTS Guidelines on myocardial revascularization: The Task Force on Myocardial Revascularization of the European Society of Cardiology (ESC) and the European Association for Cardio-Thoracic Surgery (EACTS)Developed with the special contribution of the European Association of Percutaneous Cardiovascular Interventions (EAPCI). Eur Heart J 35(37): 2541-619.

[5] G.S. Werner (2014) The role of coronary collaterals in chronic total occlusions. Curr Cardiol Rev 10(1): 57-64.

[6] R. Sachdeva, M. Agrawal, S.E. Flynn, G.S. Werner, B.F. Uretsky (2014) The myocardium supplied by a chronic total occlusion is a persistently ischemic zone. Catheter Cardiovasc Interv 83(1): 9-16.

[7] G.S. Werner, R. Surber, F. Kuethe, U. Emig, G. Schwarz, P. Bahrmann, H.R. Figulla (2005) Collaterals and the recovery of left ventricular function after recanalization of a chronic total coronary occlusion. Am

Heart J 149(1): 129-37.

[8] J.H. Choi, S.A. Chang, J.O. Choi, Y.B. Song, J.Y. Hahn, S.H. Choi, S.C. Lee, S.H. Lee, J.K. Oh, Y. Choe, H.C. Gwon (2013) Frequency of myocardial infarction and its relationship to angiographic collateral flow in territories supplied by chronically occluded coronary arteries. Circulation 127(6): 703-9.

[9] S.R. Meisel, A. Frimerman, D.S. Blondheim, A. Shotan, A. Asif, J. Shani, Y. Rozenman, M. Shochat (2013) Relation of the systemic blood pressure to the collateral pressure distal to an infarct-related coronary artery occlusion during acute myocardial infarction. Am J Cardiol 111(3): 319-23.

[10] K.P. Rentrop, M. Cohen, H. Blanke, R.A. Phillips (1985) Changes in collateral channel filling immediately after controlled coronary artery occlusion by an angioplasty balloon in human subjects. J Am Coll Cardiol 5(3): 587-92.

[11] M. Zimarino, M. D'Andreamatteo, R. Waksman, S.E. Epstein, R. De Caterina (2014) The dynamics of the coronary collateral circulation. Nat Rev Cardiol 11(4): 191-7.

[12] E.K. Economou, E. Oikonomou, G. Siasos, N. Papageorgiou, S. Tsalamandris, K. Mourouzis, S. Papaioanou, D. Tousoulis (2015) The role of microRNAs in coronary artery disease: From pathophysiology to diagnosis and treatment. Atherosclerosis 241(2): 624-33.

[13] D.A. Chistiakov, A.N. Orekhov, Y.V. Bobryshev (2016) Cardiac-specific miRNA in cardiogenesis, heart function, and cardiac pathology (with focus on myocardial infarction). J Mol Cell Cardiol 94: 107-121.

[14] H. Seitz, H. Royo, M.L. Bortolin, S.P. Lin, A.C. Ferguson-Smith, J. Cavaille (2004) A large imprinted microRNA gene cluster at the mouse Dlk1-Gtl2 domain. Genome Res 14(9): 1741-8.

[15] S.M. Welten, A.J. Bastiaansen, R.C. de Jong, M.R. de Vries, E.A. Peters, M.C. Boonstra, S.P. Sheikh, N. La Monica, E.R. Kandimalla, P.H. Quax, A.Y. Nossent (2014) Inhibition of 14q32 MicroRNAs miR-329, miR-487b, miR-494, and miR-495 increases neovascularization and blood flow recovery after ischemia. Circ Res 115(8): 696-708.

[16] P. Wang, Y. Luo, H. Duan, S. Xing, J. Zhang, D. Lu, J. Feng, D. Yang, L. Song, X. Yan (2013) MicroRNA 329 suppresses angiogenesis by targeting CD146. Mol Cell Biol 33(18): 3689-99.

[17] J.S. Esser, E. Saretzki, F. Pankratz, B. Engert, S. Grundmann, C. Bode, M. Moser, Q. Zhou (2017) Bone morphogenetic protein 4 regulates microRNAs miR-494 and miR-126-5p in control of endothelial cell function in angiogenesis. Thromb Haemost 117(4): 734-749.

[18] E.S. Brilakis, K. Mashayekhi, E. Tsuchikane, N. Abi Rafeh, K. Alaswad, M. Araya, A. Avran, L. Azzalini, A.M. Babunashvili, B. Bayani, R. Bhindi, N. Boudou, M. Boukhris, N.Z. Bozinovic, L. Bryniarski, A. Bufe, C.E. Buller, M.N. Burke, H.J. Buttner, P. Cardoso, M. Carlino, E.H. Christiansen, A. Colombo, K. Croce, F. Damas de Los Santos, T. De Martini, J. Dens, C. Di Mario, K. Dou, M. Egred, A.M. ElGuindy, J. Escaned, S. Furkalo, A. Gagnor, A.R. Galassi, R. Garbo, J. Ge, P.K. Goel, O. Goktekin, L. Grancini, J.A. Grantham, C. Hanratty, S.

Harb, S.A. Harding, J.P.S. Henriques, J.M. Hill, F.A. Jaffer, Y. Jang, R. Jussila, A. Kalnins, A. Kalyanasundaram, D.E. Kandzari, H.L. Kao, D. Karmpaliotis, H.H. Kassem, P. Knaapen, R. Kornowski, O. Krestyaninov, A.V.G. Kumar, P. Laanmets, P. Lamelas, S.W. Lee, T. Lefevre, Y. Li, S.T. Lim, S. Lo, W. Lombardi, M. McEntegart, M. Munawar, J.A. Navarro Lecaro, H.M. Ngo, W. Nicholson, G.K. Olivecrona, L. Padilla, M. Postu, A. Quadros, F.H. Quesada, V.S. Prakasa Rao, N. Reifart, M. Saghatelyan, R. Santiago, G. Sianos, E. Smith, C.S. J, G.W. Stone, J.W. Strange, K. Tammam, I. Ungi, M. Vo, V.H. Vu, S. Walsh, G.S. Werner, J.R. Wollmuth, E.B. Wu, R.M. Wyman, B. Xu, M. Yamane, L.F. Ybarra, R.W. Yeh, Q. Zhang, S. Rinfret (2019) Guiding Principles for Chronic Total Occlusion Percutaneous Coronary Intervention. Circulation 140(5): 420-433.

[19] Y. Cui, H. Chen, R. Xi, H. Cui, Y. Zhao, E. Xu, T. Yan, X. Lu, F. Huang, P. Kong, Y. Li, X. Zhu, J. Wang, W. Zhu, Y. Ma, Y. Zhou, S. Guo, L. Zhang, Y. Liu, B. Wang, Y. Xi, R. Sun, X. Yu, Y. Zhai, F. Wang, J. Yang, B. Yang, C. Cheng, J. Liu, B. Song, H. Li, Y. Wang, Y. Zhang, X. Cheng, Q. Zhan, Z. Liu (2020) Whole-genome sequencing of 508 patients identifies key molecular features associated with poor prognosis in esophageal squamous cell carcinoma. Cell Res 30(10): 902-913.

[20] B. Li, S.W. Brady, X. Ma, S. Shen, Y. Zhang, Y. Li, K. Szlachta, L. Dong, Y. Liu, F. Yang, N. Wang, D.A. Flasch, M.A. Myers, H.L. Mulder, L. Ding, L. Tian, K. Hagiwara, K. Xu, X. Zhou, E. Sioson, T. Wang, L. Yang, J. Zhao, H. Zhang, Y. Shao, H. Sun, L. Sun, J. Cai, H.Y. Sun, T.N. Lin, L. Du, H. Li, M. Rusch, M.N. Edmonson, J. Easton, X. Zhu, J. Zhang, C. Cheng, B.J. Raphael, J. Tang, J.R. Downing, L.B. Alexandrov, B.S. Zhou, C.H. Pui, J.J. Yang (2020) Therapy-induced mutations drive the genomic landscape of relapsed acute lymphoblastic leukemia. Blood 135(1): 41-55.

[21] W. Gao, H. Liu, J. Yuan, C. Wu, D. Huang, Y. Ma, J. Zhu, L. Ma, J. Guo, H. Shi, Y. Zou, J. Ge (2016) Exosomes derived from mature dendritic cells increase endothelial inflammation and atherosclerosis via membrane TNF-alpha mediated NF-kappaB pathway. J Cell Mol Med 20(12): 2318-2327.

[22] K.J. Livak, T.D. Schmittgen (2001) Analysis of relative gene expression data using real-time quantitative PCR and the 2(-Delta Delta C(T)) Method. Methods 25(4): 402-8.

[23] Y. Bai, R. Liu, Z. Li, Y. Zhang, X. Wang, J. Wu, S. Qian, B. Li, Z. Zhang, A.H. Fathy, D. Cappetta, J. Zhou, Y. Zou, J. Qian, J. Ge (2019) VEGFR endocytosis regulates the angiogenesis in a mouse model of hindlimb ischemia. J Thorac Dis 11(5): 1849-1859.

[24] C. Li, R. Xu, K. Yao, J. Zhang, S. Chen, L. Pang, H. Lu, Y. Dai, J. Qian, H. Shi, J. Ge (2020) Functional significance of intermediate coronary stenosis in patients with single-vessel coronary artery disease: A comparison of dynamic SPECT coronary flow reserve with intracoronary pressure-derived fractional flow reserve (FFR). J Nucl Cardiol: Online ahead of print.

[25] W.J. Stuijfzand, R.S. Driessen, P.G. Raijmakers, M.T. Rijnierse, J. Maeremans, M.R. Hollander, A.A. Lammertsma, A.C. van Rossum, J. Dens, A. Nap, N. van Royen, P. Knaapen (2017) Prevalence of

ischaemia in patients with a chronic total occlusion and preserved left ventricular ejection fraction. Eur Heart J Cardiovasc Imaging 18(9): 1025-1033.

[26] Q. Qin, J. Qian, J. Ma, L. Ge, J. Ge (2016) Relationship between thrombospondin-1, endostatin, angiopoietin-2, and coronary collateral development in patients with chronic total occlusion. Medicine (Baltimore) 95(33): e4524.

[27] M. Sahin, S. Demir, M.E. Kalkan, B. Ozkan, G. Alici, K.C. Cakalagaoglu, M.V. Yazicioglu, S. Sarikaya, M. Biteker, M.M. Turkmen (2014) The relationship between gamma-glutamyltransferase and coronary collateral circulation in patients with chronic total occlusion. Anadolu Kardiyol Derg 14(1): 48-54.

[28] A.B. Nacar, A. Erayman, M. Kurt, E. Buyukkaya, M.F. Karakas, A.B. Akcay, S. Buyukkaya, N. Sen (2015) The relationship between coronary collateral circulation and neutrophil/lymphocyte ratio in patients with coronary chronic total occlusion. Med Princ Pract 24(1): 65-9.

[29] M. Kalkan, M. Sahin, A. Kalkan, A. Guler, M. Tas, M. Bulut, S. Demir, R. Acar, U. Arslantas, B. Ozturkeri, Y. Guler, M. Akcakoyun (2014) The relationship between the neutrophil-lymphocyte ratio and the coronary collateral circulation in patients with chronic total occlusion. Perfusion 29(4): 360-366.

[30] E. Sogut, H. Kadi, M. Karayakali, C. Mertoglu (2015) The association of plasma vitamin A and E levels with coronary collateral circulation. Atherosclerosis 239(2): 547-51.

[31] Y. Shen, F.H. Ding, R.Y. Zhang, Q. Zhang, L. Lu, W.F. Shen (2016) Association of serum mimecan with angiographic coronary collateralization in patients with stable coronary artery disease and chronic total occlusion. Atherosclerosis 252: 75-81.

[32] K.M. Gurses, M.U. Yalcin, D. Kocyigit, M.S. Besler, H. Canpinar, B. Evranos, H. Yorgun, M.L. Sahiner, E.B. Kaya, N. Ozer, D. Guc, K. Aytemir, L. Tokgozoglu (2019) The association between serum angiogenin and osteopontin levels and coronary collateral circulation in patients with chronic total occlusion. Anatol J Cardiol 22(2): 77-84.

[33] N. Hakimzadeh, A.Y. Nossent, A.M. van der Laan, S.H. Schirmer, M.W. de Ronde, S.J. Pinto-Sietsma, N. van Royen, P.H. Quax, I.E. Hoefer, J.J. Piek (2015) Circulating MicroRNAs Characterizing Patients with Insufficient Coronary Collateral Artery Function. PLoS One 10(9): e0137035.

[34] D. Kir, E. Schnettler, S. Modi, S. Ramakrishnan (2018) Regulation of angiogenesis by microRNAs in cardiovascular diseases. Angiogenesis 21(4): 699-710.

[35] K. Fitzgerald, S. White, A. Borodovsky, B.R. Bettencourt, A. Strahs, V. Clausen, P. Wijngaard, J.D. Horton, J. Taubel, A. Brooks, C. Fernando, R.S. Kauffman, D. Kallend, A. Vaishnaw, A. Simon (2017) A Highly Durable RNAi Therapeutic Inhibitor of PCSK9. N Engl J Med 376(1): 41-51.

[36] M.S. Sabatine, R.P. Giugliano, A.C. Keech, N. Honarpour, S.D. Wiviott, S.A. Murphy, J.F. Kuder, H. Wang, T. Liu, S.M. Wasserman, P.S. Sever, T.R. Pedersen (2017) Evolocumab and Clinical Outcomes in Patients

with Cardiovascular Disease. N Engl J Med 376(18): 1713-1722.

[37] U.K. Allahwala, J. Weaver, R. Bhindi (2019) Animal chronic total occlusion models: A review of the current literature and future goals. Thromb Res 177: 83-90.

[38] D. Sun, J. Wang, Y. Tian, K. Narsinh, H. Wang, C. Li, X. Ma, Y. Wang, D. Wang, J.C. Wu, J. Tian, F. Cao (2012) Multimodality imaging evaluation of functional and clinical benefits of percutaneous coronary intervention in patients with chronic total occlusion lesion. Theranostics 2(8): 788-800.

Figures

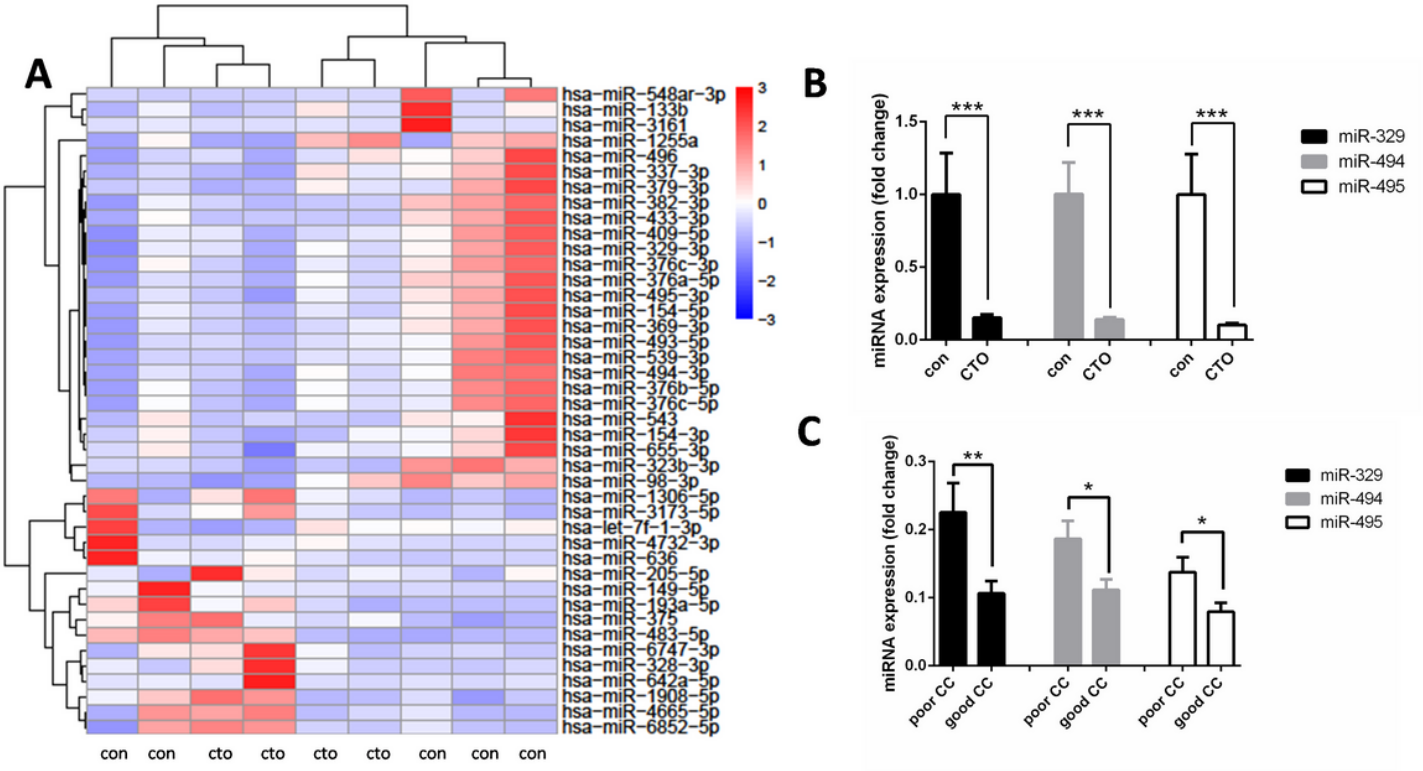

Figure 1

Profiling and identification of differentially expressed miRNAs in plasma from patients with coronary artery disease (control group) and chronic total occlusions (CTO group). A, Heatmap and hierarchical clustering of the top 42 miRNAs with differential expression levels of >2.5-fold across all samples. B, Expressions of miR-329, miR-494 and miR-495 in control group (N=22) and CTO group (N=46). C, Patients in CTO group were divided into 2 subgroups according to CC grade. Expressions of miR-329, miR-494 and miR-495 in poor CC group (N=17, CC=0 or 1) and good CC group (N=27, CC=2) . *P<0.05, **P<0.01, *** P<0.001.

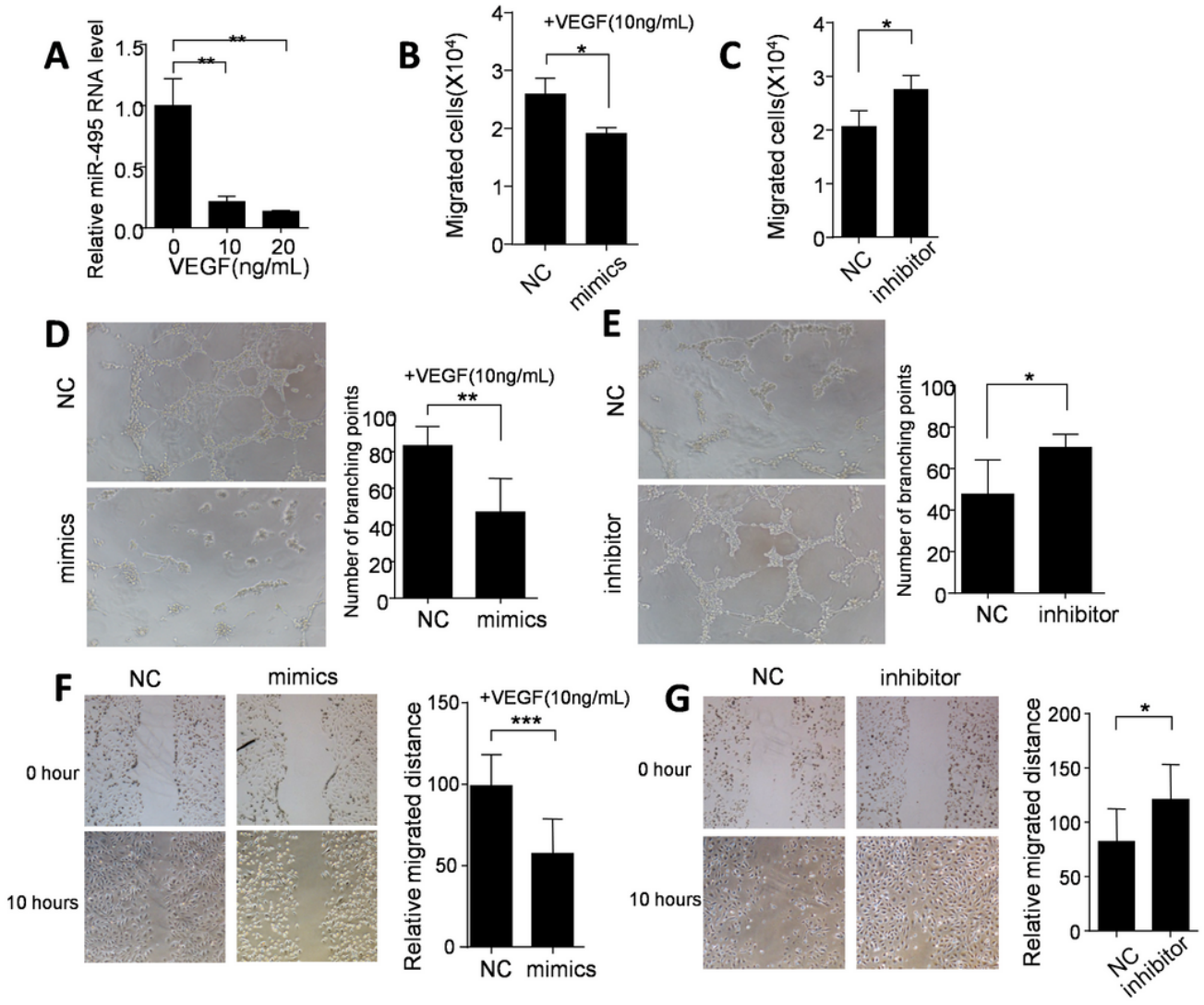

Figure 2

Role of miR-495 in angiogenesis of human umbilical vein endothelial cells (HUVECs). A, mR-495 expression determined by RT-PCR in HUVECs treated with different concentrations of vascular endothelial growth factor (VEGF) for 24h. B, HUVECs were transfected with miR-495 NC (50nM) or mimics (50nM) for 36h and then cells (1*10^5 cells per well) were seeded into the upper chamber added with VEGF (10ng/ml). The invasive cells were harvested after incubation for 48h. C, HUVECs were transfected with miR-495 NC or inhibitor (100nM) for 36h and then cells were seeded into the upper chamber added without VEGF. The invasive cells were harvested after incubation for 48h. D, HUVECs were transfected with miR-495 NC or mimics for 36h. Then cells were cultured with VEGF (10ng/ml) and microscopically recorded for the formation of tube-like structures 8h later. E, HUVECs were transfected with miR-495 NC or inhibitor for 36h. Then cells were cultured without VEGF and microscopically recorded for the formation of tube-like structures 8h later. F. HUVECs were transfected with miR-495 NC or mimics for 36h. Then cells were cultured with VEGF (10ng/ml) and wound healing assay was performed 10h after scratch. G, HUVECs were transfected with miR-495 NC or inhibitor for 36h. Then cells were cultured without VEGF and wound healing assay was performed 10h after scratch. *P<0.05, **P<0.01, *** P<0.001.

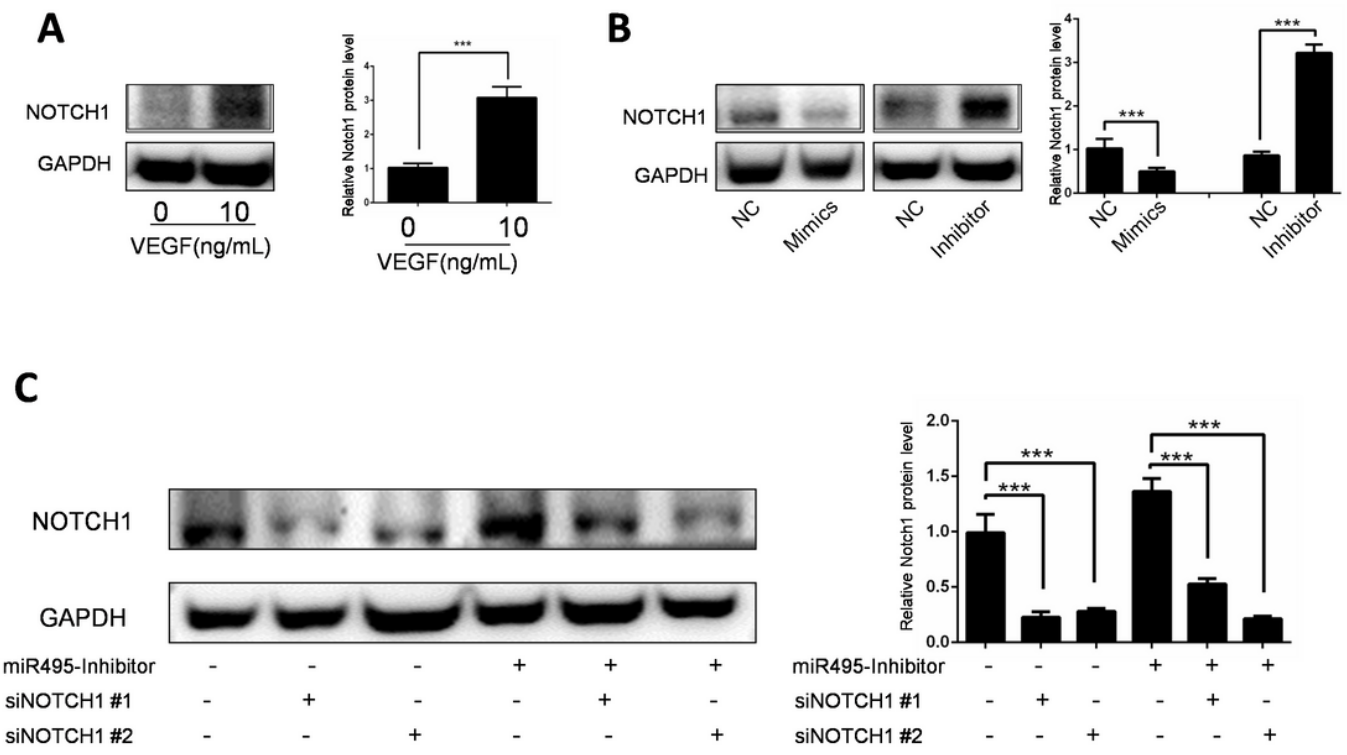

Figure 3

miR-495 targets Notch1 in HUVECs. A, HUVECs were cultured with VEGF (10ng/ml) for 24h and protein level of Notch1 was determined by WB. B, HUVECs were cultured miR-495 NC (50nM), mimics (50nM) or inhibitors (100nM) for 48h and protein level of Notch1 was determined. C, HUVECs were cultured with miR-495 inhibitor or not. Then siNotch1 #1 or #2 (50nM) was added into medium and protein level of Notch1 was determined after 48h. *** P<0.001.

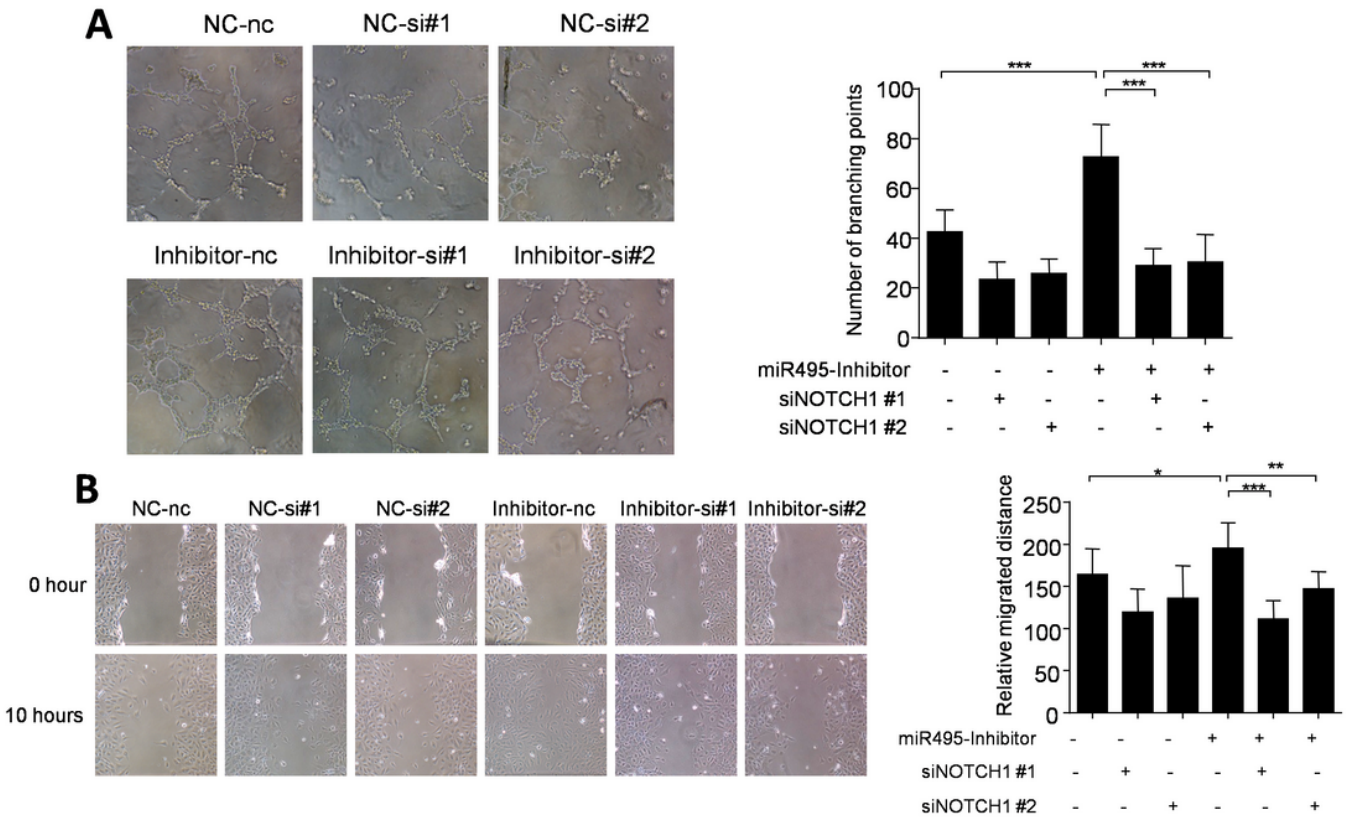

Figure 4

Notch1 was involved in miR-495 inhibitor induced angiogenesis. A-B, HUVECs were cultured with miR-495 inhibitor (100nM) or not. And siNotch1 NC, #1 or #2 was added at a concentration of 50nM. Formation of tube-like structures was recorded 8h later (A). Wound healing assay was performed 10h after scratch (B). *P<0.05, *** P<0.001.

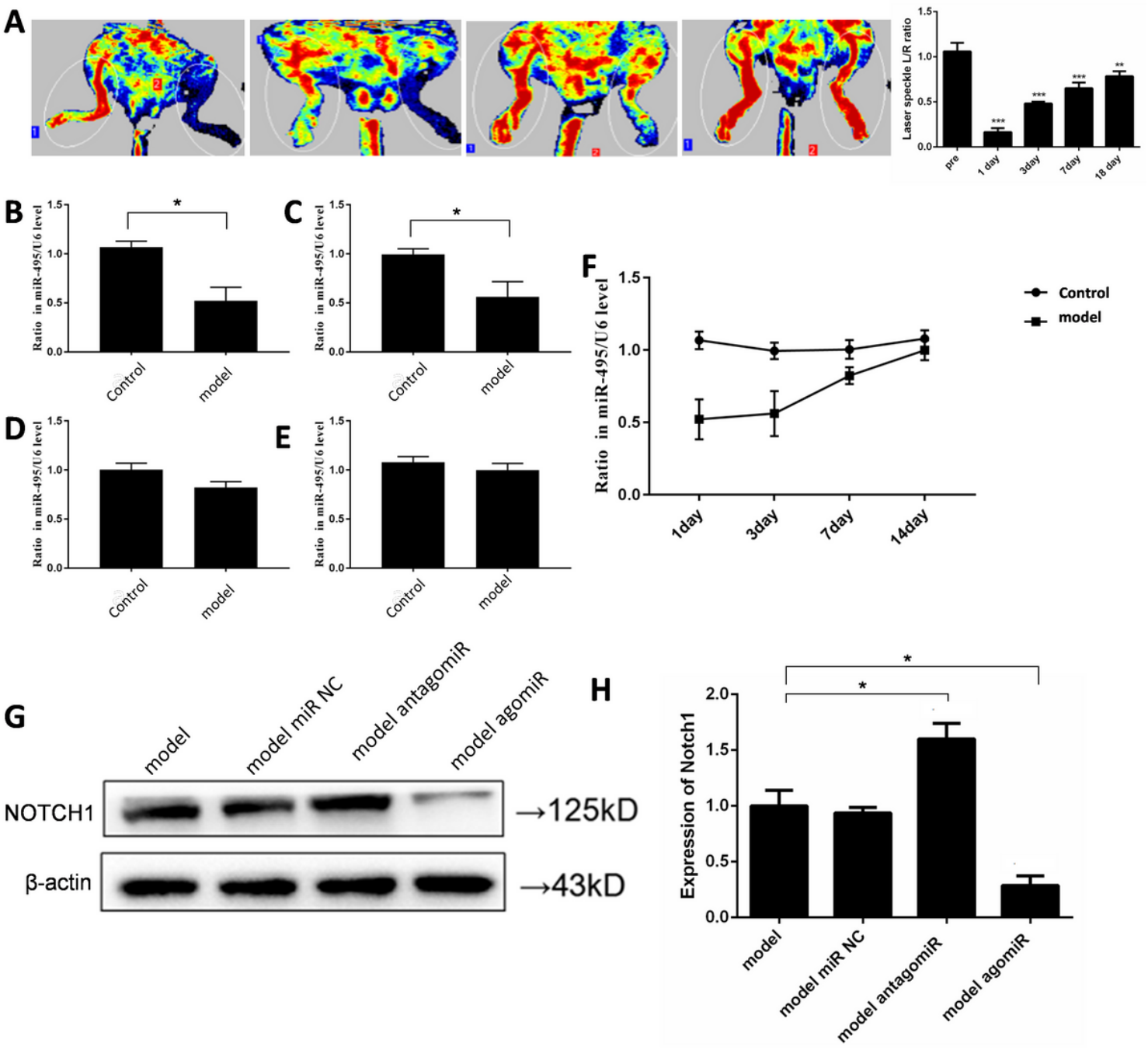

Figure 5

Notch1 was the target of miR-495 in mice hindlimb ischemia model. A, Representative pictures of blood flow in mice hindlimbs. Left femoral artery of mice was ligated and limb perfusion was assessed at day 1, 3, 7, and 18 by laser Doppler perfusion imaging. B-F, After hindlimb ischemia of mice, expression of miR-495 in plasma was detected at day 1 (B), 3 (C), 7 (D) and 14 (E). A gradual recovery of miR-495 expression was also showed (F). G-H, After ligation, miR-495 NC (5nM), antago (10nM) and ago (5nM) were injected into ischemic muscle every other day. Then we detected expression of Notch1 protein at day 3. N=5 mice in each group. *P<0.05, **P<0.01, *** P<0.001.

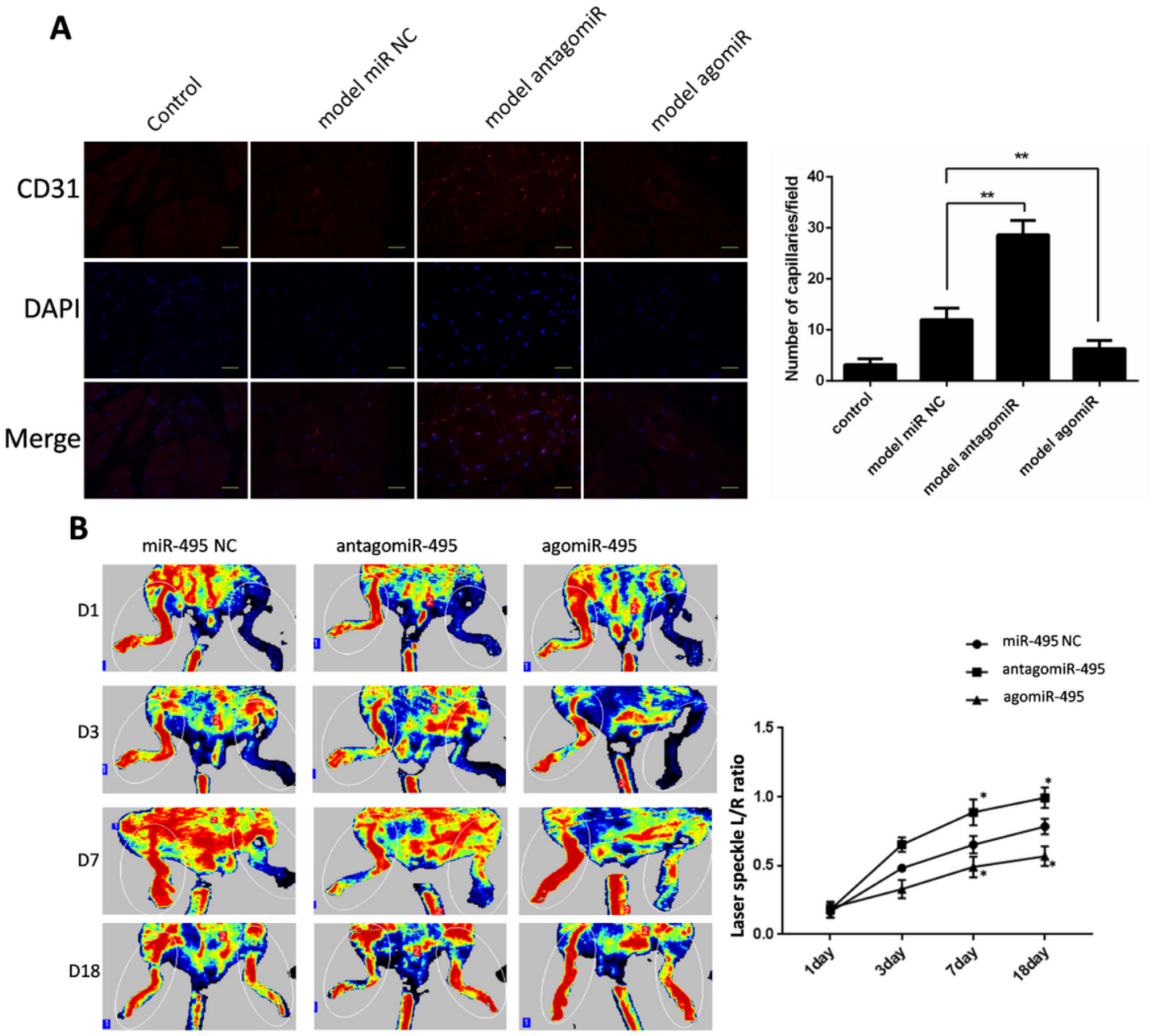

Figure 6

Angiogenesis and collateral formation in hindlimb ischemia model. A, Representative immunofluorescence assay pictures of mice adductor muscle. After ligation, miR-495 NC (5nM), antago (10nM) and ago (5nM) were injected into ischemic muscle. The adductor muscles were harvested at the 3rd day after femoral ligation. CD31 and DAPI were stained. B, Representative pictures of blood flow in mice hindlimbs. Left femoral artery of mice was ligated and miR-495 NC, antago and ago were injected into ischemic muscle. Limb perfusion was assessed at day 1, 3, 7, and 18 by laser Doppler perfusion imaging. N=5 mice in each group. *P<0.05, **P<0.01, *** P<0.001.

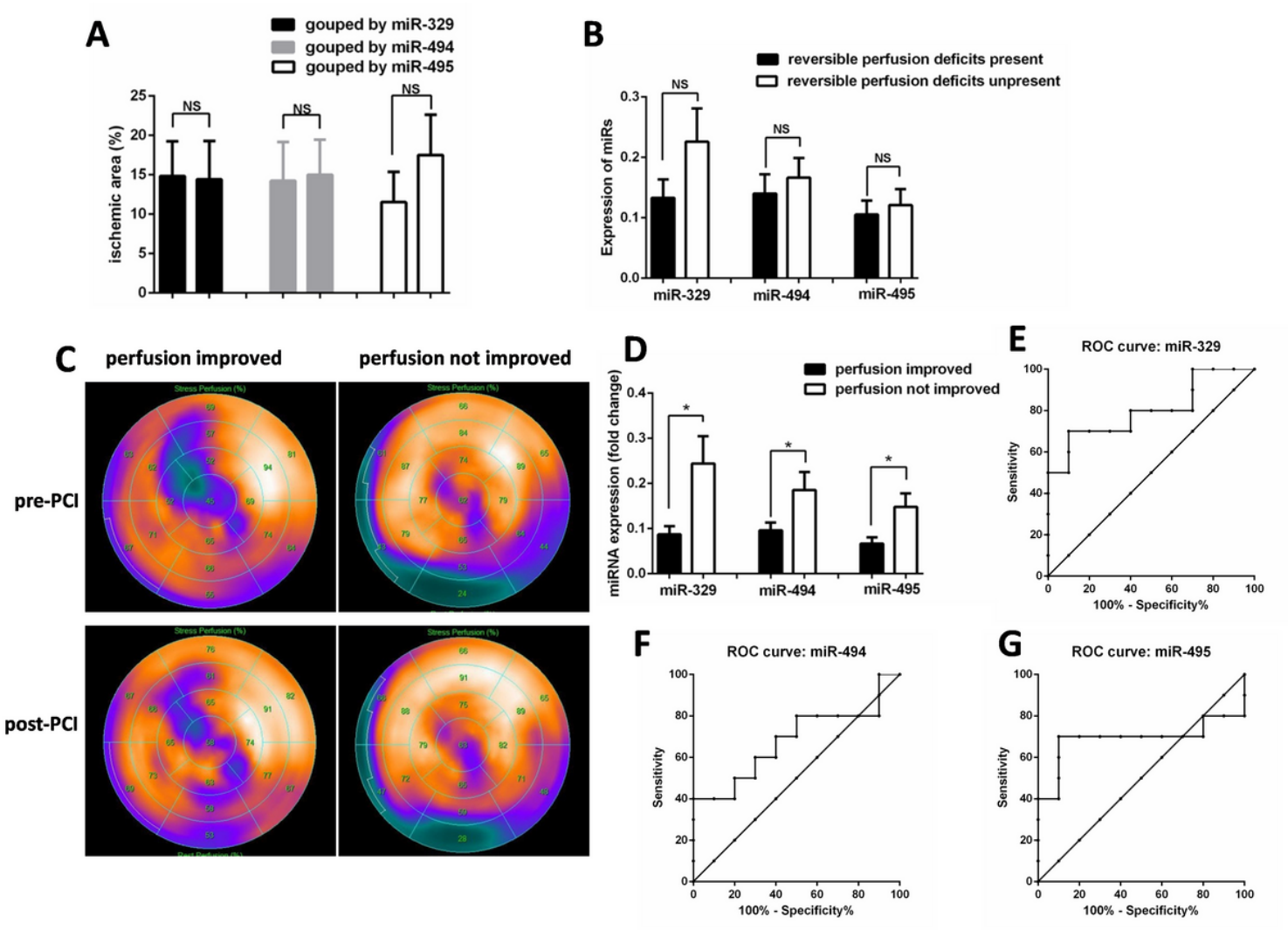

Figure 7

Association between 3 miRs and myocardial perfusion assessed by PSECT. A, A total of 27 patients underwent SPECT and were divided into 2 groups according to expression of miR-329, miR-494 and miR-495. The ischemia area was compared between groups. B, These 27 patients were divided into 2 groups according to whether reversible perfusion deficits present. Expression of miR-329, miR-494 and miR-495 was compared between groups. C, A total of 20 patients underwent a second SPECT after successful revascularization of occluded artery. Representative images of patients with improved (left panel) or not improved (right panel) perfusion after revascularization. D, These 20 patients were divided into 2 groups according to whether myocardial perfusion was improved. Expression of miR-329, miR-494 and miR-495 was compared between groups. E-G, Receiver operating characteristic (ROC) analysis of miR-329, miR-494, and miR-495 to predict whether patients can obtain improved myocardial perfusion after revascularization. The area under the curve (AUC) was 0.80, 0.68 and 0.69, respectively. *P<0.05.